RSC Advances

PAPER

View Article Online
View Journal | View Issue

Cite this: *RSC Adv.*, 2020, **10**, 44774

Monohydrate and anhydrate of nylon 5I monomer 1,5-pentanediamine–isophthalate†

Zihan Li,[a] Mengjie Xu,[a] Haodong Liu,[a] Qingshi Wen,[b] Jinqiu Fu,[c] Wei Zhuang,[a] Pengpeng Yang,*[a] Jinglan Wu[a] and Hanjie Ying[a]

Nylon 5I is one of the new bio-based nylon materials. Its raw material 1,5-pentanediamine (PDA) is prepared by biological methods using biomass as the raw material. The high-performance polymer materials require the original high-quality monomers. 1,5-Pentanediamine–isophthalate (PDA–IPA) was taken as the direct monomer for the preparation of nylon 5I, and the crystallization was a valuable and essential approach to preparing the good-performance monomer salt. In this report, we found and obtained two crystal forms of PDA–IPA, monohydrate and an anhydrous form. Their crystal structures were determined and analyzed by single crystal X-ray diffraction (SCXRD), powder X-ray diffraction (PXRD), and Fourier transform infrared spectroscopy (FTIR). Hirshfeld surface maps were employed to capture the differences in the interactions present in the two forms. The thermal behaviors were characterized by differential scanning calorimetry (DSC) and thermogravimetric analysis (TGA). Moreover, the monohydrate and anhydrous phase can transform to each other through solid–solid transformation or solution-mediated phase transformation, and the critical values of the phase transformation were determined. Finally, the relative stability of the two forms under different thermodynamic conditions was discussed, especially the influence of temperature and water activity on the stability.

Received 15th October 2020
Accepted 11th November 2020

DOI: 10.1039/d0ra08767j

rsc.li/rsc-advances

Introduction

Nylon, also called polyamide (PA), is the general name of thermoplastic resins containing repeating amide groups on the molecular backbone, with excellent mechanical properties, such as friction resistance, self-lubricity, acid and alkali resistance. With the increasing requirements for plastic materials in the fields of electronics, automobiles, aerospace, and chemical industry, the market demand for high-temperature resistant nylon with superb performance has expanded dramatically.[1] High melting temperature and heat resistance are the main advantages of semi-aromatic polyamides, such as PA4T/4I/6T, which has low cost and moderate water absorption rate, and has been brought on the market as the high-temperature resistant nylon material.[2–4] However, the extraction and production of their raw materials involve related toxic chemical substances, which has caused serious damage and pollution to the environment.[5,6]

In recent years, new bio-based nylons based on crops and other biomass resources have become a new research hotspot in the nylon industry due to its consistency with the national sustainable development concept.[7] Since the raw materials can achieve sustainability in the production and preparation process, it is considered to be a new trend leading the direction of future material development.[8] The bio-nylon series based on 1,5-pentanediamine (PDA) is opening up a green route for nylon production attributed to its good industry applications.[9,10] Nylon 5I, which is polymerized by 1,5-pentanediamine–isophthalate (herein after referred to as PDA–IPA, see Fig. 1, $C_{13}H_{20}N_2O_4$, MW 268.33 g mol^{-1}), is considered to be a potential substitute of the traditional nylon 4I/4T/6T for its high-temperature resistance. As we all know, high-quality monomers are essential to synthesize excellent performance polymers, and the crystallization was taken as the main method for

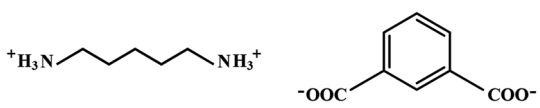

Fig. 1 Molecular structure of 1,5-pentanediamine–isophthalate.

[a]National Engineering Technique Research Center for Biotechnology, State Key Laboratory of Materials-Oriented Chemical Engineering, Jiangsu Synergetic Innovation Center for Advanced Bio-Manufacture, College of Biotechnology and Pharmaceutical Engineering, Nanjing Tech University, No. 30, Puzhu South Road, 211816 Nanjing, China. E-mail: yang-pengpeng@njtech.edu.cn

[b]Industrial Biotechnology Institute of Jiangsu Industrial Technology Research Institute, 211816 Nanjing, China

[c]School of Chemical Engineering, Zhengzhou University, Zhengzhou, 450001, China

† Electronic supplementary information (ESI) available. CCDC 1969111 and 1969113. For ESI and crystallographic data in CIF or other electronic format see DOI: 10.1039/d0ra08767j

the preparation and purification of monomers.[11,12] During our research, we found that PDA–IPA exists in two crystal forms, one contains crystal water and the other does not.

It is common that compounds exists in both hydrate and anhydrous forms,[13] especially for bio-chemicals involving water as the solvent in their preparation process.[14] The hydrates of a compound may well have different physicochemical properties compared to its parent anhydrate forms, such as solubility, density, hygroscopicity, dissolution rate, chemical stability, and mechanical property.[15–20] Therefore, investigating the hydration state, possible transformation pathways and mechanism under different conditions is very helpful to guarantee the product quality.[21,22]

Given that the transportation, use, and storage of the product were significantly influenced by the stability,[23] it is necessary to understand the relative stability of different solid forms, especially to find the optimum crystal forms of the target compounds. Related studies on theophylline, ampicillin and naproxen sodium indicate that the water activity (a_w) in the experimental system using mixed solvents is the key factor in determining the mutual transition between hydrate and anhydrate.[24–26] For a given temperature, there exists a corresponding equilibrium value of water activity, the relative stability of the anhydrous and hydrated forms is consistent at this time. Besides, any fluctuation in the equilibrium water activity under the same conditions may lead to a phase transformation.

Solid-state transformations (SST)[27–30] and solution-mediated polymorphic transformations (SMPT) are two common mechanism of the phase transformation.[30–35] The SMPT process is more common than the former, mainly because most of the polymorphic conversion process occurs in the solvent systems. Slurry experiments are a special type in the SMPT category. Considering its simplicity and ease of operation, it is often used to screen the polymorphs of the crystal products and to evaluate the relative stability of different forms. Many research cases have shown that the water activity is the major factor in the hydration of the compound in the slurry experiments with water–solvent mixtures.[24,36]

In this research, the two crystalline powders of the PDA–IPA were characterized from their structures, morphology, stability, and thermal behaviors by SCXRD, PXRD, FTIR, and TGA-DSC. The differences in the crystal structure, hydrogen-bonding interactions, and molecular packing between the monohydrate and anhydrate have also been investigated based on the single crystal data and Hirshfeld surface analysis. Moreover, phase transformations between the two forms under different thermodynamic and humidity conditions were studied through the SST and SMPT experiments, and the transformation mechanism of the two solid forms was finally elucidated.

Experimental section

Materials

1,5-Pentanediamine (PDA, 99.5% purity, mp 180 °C, MW 102.18 g mol^{-1}) was prepared by the biological method of L-lysine decarboxylation in our laboratory. Its purity and concentration were determined by high performance liquid chromatography (HPLC). Analytical-grade ethanol (EtOH, 99.5% purity, bp 78.3 °C, MW 46.07 g mol^{-1}) was obtained from Shanghai Chemistry Reagent Co. (China). Isophthalic acid (IPA, 99.5% purity, mp 341 °C, MW 166.13 g mol^{-1}) was purchased from Shanghai Macklin Biochemical Co., Ltd. Deionized water was obtained from an ultrapure water system (YPYD CO., China).

Preparation of the crystal forms

The PDA–IPA monohydrate was prepared by ethanol anti-solvent crystallization in aqueous solution. A total of 3.6 ± 0.1 g of the PDA was dissolved in 10 g of water in a 50 ml beaker first, and then poured into a 100 ml double-jacketed crystallizer at ambient temperature. The solution was agitated by a stirrer with three blades at 200 rpm (HD2015W, Sile Instrument, China). After complete mixing, 5.85 g IPA powder was added in batches into the aqueous solution of PDA, and was continuously stirred until the mixed solution became transparent. Ethanol was chosen as the anti-solvent, and was added to the mixed solution at a constant rate of 1.0 ml min^{-1} using a peristaltic pump (model BT100-1L, Baoding Longer, China). The total amount of the anti-solvent added was ten times that of the solvent. Precipitation gradually appeared with the addition of EtOH after about 20 min, and the system was kept stirring for 2 h to obtain crystals.

The anhydrous form of PDA–IPA was prepared by reaction crystallization. 3.6 ± 0.1 g of the PDA was completely dissolved in 50 ml of EtOH at room temperature. 100 ml of ethanol was poured into a 250 ml double-jacketed crystallizer at 45 °C (controlled by a temperature circulation pump, CK-4005GD, SCIENTZ). Then, 5.85 g of the IPA solid powder was slowly added to the crystallizer, and the solution was agitated at 200 rpm for 2 hours. The liquid was transparent after the IPA completely dissolved in EtOH, and then the mixed PDA–EtOH solution was slowly pumped into the jacket using a peristaltic pump at a constant rate of 0.8 ml min^{-1}. The nucleation of the crystal was observed about 15 minutes after adding the PDA–EtOH. The system was held at a constant temperature, and the crystals were obtained after stirring for 2 hours.

After filtering, washing with EtOH, and air-drying in a vacuum oven at 40 °C for 12 hours, we finally obtained the two crystalline products. The structures of the sample were identified by PXRD for consistency.

Transformation experiments

SST process between the monohydrate and anhydrate. The conversion relationship of the two crystal forms under different thermal and humidity conditions was studied. The first factor investigated was humidity. About 200 mg of crystalline powder was taken of the two forms, and placed in Petri dishes with a 5 cm diameter of varying relative humidity (RH = ~0%, 32%, 43%, 67%, 76%, 98%).[37] After being placed at room temperature for 6 weeks, the samples were taken out and characterized by PXRD. Meanwhile, we also investigated the hygroscopicity of the two crystal forms by tracing the mass variation of the samples subjected to different humidity circumstances.

Temperature was the second factor to be considered. About 200 mg powder of the two crystal forms was weighted in several dishes, stored at room temperature, 40 °C, 60 °C, 80 °C for one month, and at 120 °C for 15 h. Samples were also identified by PXRD after the test period.

SMPT process between the monohydrate and anhydrate. Five solvents (methanol, ethanol, water, water–2-propanol and water–ethanol) were used to screen for the PDA–IPA polymorphs and phase transformation. Saturated solutions of PDA–IPA were put in a 25 ml triangular conical flask, and stirred using a rotor at 500 rpm. An excessive amount of the two crystal forms of PDA–IPA powder was added to different mixed solvents, and agitated at certain temperatures for 2 weeks. The turbid liquid was filtered after the experiments. The obtained filter cake was dried, and then characterized by PXRD.

Slurry experiments. By slurrying the two crystalline powders in the water–ethanol binary solvents with various water activities, the critical water activity required for the hydration of the two forms was determined.[38] Furthermore, when the experiments were performed at various temperatures, different critical water activities were obtained. In this work, the experimental temperatures were 293.15, 298.15, 303.15, 308.15 in 5 K increments to 343.15 ± 0.1 K, and the water activity was calculated by the Margules formula.[24] A series of binary mixtures composed of water and ethanol (water mole fractions $X_w = 0.02, 0.06, 0.1, 0.15, 0.2, 0.3$ in 0.1 increments to 1.0) were prepared. The excess of the two crystalline powders was added into about 8 ml of the mixed solvents, and stirred well for 24 h to reach a solid–liquid two-phase equilibrium. After filtering the mixed solution, the wet cakes were taken out and identified by PXRD as well.

Single crystal X-ray diffraction (SCXRD)

A single crystal of the monohydrate was obtained in pure water by cooling crystallization, while the anhydrate was obtained in a pure ethanol solution by evaporation crystallization. The specific method of evaporation crystallization is to add a slight excess of crystalline powder of the anhydrate to a 20 ml beaker containing 15 ml water–ethanol binary solvent (95% wt ethanol content). After it was stirred thoroughly and the solid was completely dissolved, the beaker is placed into another 100 ml beaker filled with 30 ml DMF solvent. The large beaker was tightly sealed, and then the anhydrous single crystal slowly precipitated out after 1 week.

The single-crystal structures were determined on a Bruker SMART APEX diffractometer using Mo Kα radiation (λ = 0.71073 Å) with a graphite monochromator at room temperature. The Bruker SMART-1000 program was used for data collection. The integration and scaling of the intensity data were accomplished using the SAINT[39] program. The structures were analyzed by direct methods, and refined by full matrix least-squares methods on F^2.[40] All of the hydrogen atoms were treated by a constrained refinement, including the ones connected to amidogen and carboxylic group, and were located in a difference Fourier map with bond-length restraints of N–H = 0.89(1) Å. All non-hydrogen atoms were refined with anisotropic thermal parameters, and calculations were implemented by the SHELXL-2018/3.[41] The measurement details of the diffraction and refinements are shown in Table 1, and the data was processed using PLATON.[42] MERCURY 3.3 [43] was used for structure visualization, and the acquisition of standard diffraction patterns.

Fourier transform infrared spectroscopy (FTIR)

Infrared spectra of the products were recorded on a FT-IR spectrometer (Nicolet iS5, Thermo Scientific, USA) with an ATR reflectance attachment. Spectra were collected in the wavenumber range of 4000–500 cm^{-1} with a resolution of 4 cm^{-1}.

Powder X-ray diffraction (PXRD)

PXRD is an advantageous tool for the qualitative identification of crystalline powder. In this work, PXRD patterns were obtained using a Rigaku SmartLab diffractometer system using Cu Kα radiation (λ = 1.5406 Å). The intensity data were collected at 150 K. The sample was scanned within the 2θ range from 5° to 40° in continuous scan mode, with a rate of 10° min^{-1} and a step size of 0.02°. The experimental PXRD patterns of the samples were compared with those calculated from their single-crystal structures.

Thermogravimetry and differential scanning calorimetry (TGA-DSC)

TGA-DSC (NETZSCH STA 449 F3, NETZSCH, Germany) was conducted to characterize the thermal behaviors of the PDA–IPA

Table 1 Crystallographic data for the PDA–IPA monohydrate and anhydrous form

	Monohydrate	Anhydrate
Empirical formula	$C_{13}H_{20}N_2O_4 \cdot H_2O$	$C_{13}H_{20}N_2O_4$
Formula weight	286.33	268.33
Crystal system	Orthorhombic	Monoclinic
Space group	*Pbcn*	$P2_1/n$
a (Å)	10.9462(9)	13.4758(12)
b (Å)	13.6297(11)	11.6629(11)
c (Å)	19.4386(16)	18.8817(16)
α (deg)	90	90
β (deg)	90	103.974(4)
γ (deg)	90	90
Volume ($Å^3$)	2900.1(4)	2879.8(4)
Z	8	8
$D_{calc.}$ (g cm^{-3})	1.312	1.238
μ (mm^{-1})	0.101	0.092
F (000)	1232	1152
Crystal size (mm)	0.15 × 0.27 × 0.40	0.10 × 0.30 × 0.37
Observed data [$I > 2\sigma(I)$]	1764	2581
R(int)	0.046	0.088
R_1 [$I > 2\sigma(I)$]	0.0397	0.0646
wR^2	0.1104	0.1324
GOF on F^2	1.02	1.03
Diff. density (e $Å^{-3}$)	−0.20, 0.16	−0.20, 0.23
CCDC	1969111	1969113

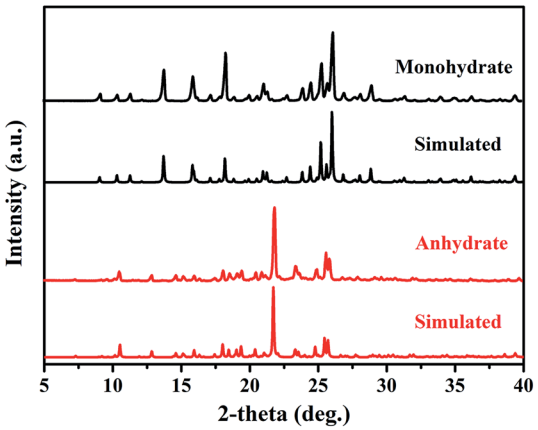

Fig. 2 Comparison of powder X-ray diffraction (PXRD) patterns with the simulated patterns from single-crystal X-ray diffraction (SCXRD) for the monohydrate and anhydrate of PDA–IPA.

monohydrate and anhydrous crystals. Approximately 20 mg of the sample was added to an alumina crucible, and purged with a stream of flowing nitrogen throughout the experiment at 40 ml min^{-1}. The heating rate was 10 °C min^{-1} and the temperature range was between 25 and 500 °C.

Hirshfeld surface analysis (HSs)

Molecular HSs analysis[44] and fingerprint plots of the two crystal forms of PDA–IPA were performed using the CrystalExplorer 17.5 software to gain further insight into the packing modes and intermolecular interactions in crystals.[45,46]

Results and discussion

PXRD analysis

The PDA–IPA hydrate and its anhydrous phase were characterized by PXRD to ensure phase identity (Fig. 2). The two crystal forms have their individual characteristic peaks: the peaks of the monohydrate were detected at 13.76°, 18.24°, 25.24° and 26.06° (2θ), while those of the anhydrate were located at 21.72°, 25.46° and 25.72° (2θ). The PXRD fingerprint of the two forms can be easily distinguished, and the experimental patterns coincide well with the simulated ones calculated from their single-crystal structures. In fact, it was found that it was also easy to distinguish them by their morphology: rod-like for the monohydrate and block-like for the anhydrate, as illustrated in Fig. 3.

Crystal structures analysis

Crystallographic details of the two crystal forms are listed in Table 1. There exists eight molecules in the unit cells for both crystal forms of PDA–IPA (Fig. S1 and S2†), and the PDA and IPA exist as a protonation and deprotonation state in the two crystal lattices, respectively. In fact, the proton transfer was completed in aqueous solution before the crystallization. Meanwhile, it was revealed that there are considerable structural differences between the two forms of PDA–IPA. The monohydrate is an orthorhombic system, *Pbcn* space group, while the anhydrate is monoclinic, $P2_1/n$ space group. There exist eight molecules for both crystalline forms in the unit cell (Fig. S1 and S2†). The monohydrate contains one crystal water molecule, while the anhydrate does not. The crystal density of the monohydrate was 1.312 g cm^{-3}, which is higher than that of the anhydrous form at 1.238 g cm^{-3}.

Compared to the asymmetric unit in the crystal structure of the monohydrate, that of the anhydrous form contains a pair of PDA–IPA species. A huge twist of the single PDA molecule in the crystal lattice is a significant feature of the conformational difference between the two forms, reflecting the difference of the torsion angles of the PDA species: C11–C12–C13–N2 (−178.68°) for the monohydrate, in comparison with C19–C20–C21–N2 (−174.28°) and C23–C24–C25–C26 (66.05°) for the anhydrate (shown in Fig. 4a and b). The phenomenon was mainly caused by the different intermolecular interactions of the host molecules (see details of the hydrogen bonds data and torsion angles in Tables S1 and S2†). The carbon chain of another PDA species in the anhydrate shows a big twist, making it tightly connect to the adjacent IPA and PDA molecules. It should be pointed out that such conformation rotation never appeared in the nylon 54 salt\56 salt\5T salt (monomer) reported in our previous research.[47–49]

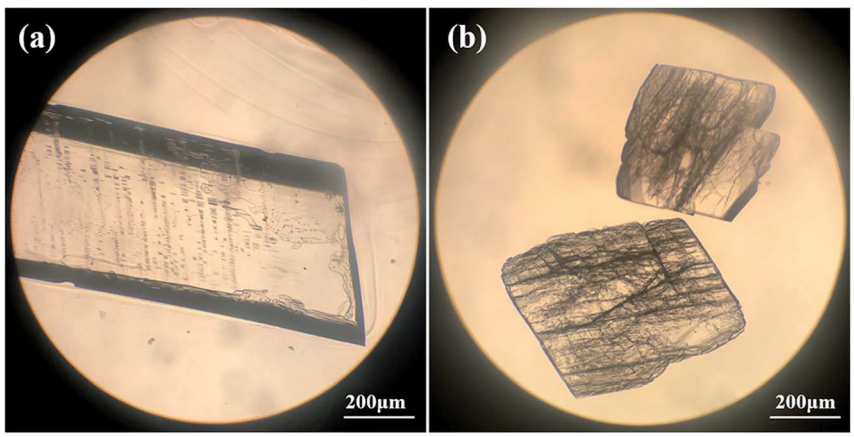

Fig. 3 Optical micrographs of crystals obtained in experiments: (a) monohydrate; (b) anhydrous form. The magnifications are 16× 10.

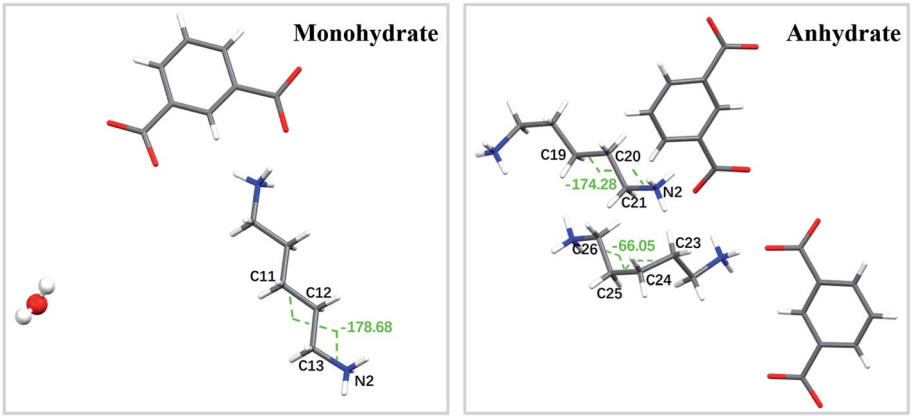

Fig. 4 The conformational difference between the monohydrate (a) and anhydrate (b) of PDA–IPA.

The structures of the PDA–IPA monohydrate and anhydrate show different packing modes along the *b* axis, as shown in Fig. 5. There are two types of hydrogen-bond contact, N–H···O and O–H···O, in the monohydrate. In Fig. 5a, the H atom of the amino group of PDA is bonded with the O atom of the carboxyl group of IPA by hydrogen bond interaction. Moreover, the water molecule acts as a bridge to connect two adjacent IPA molecules that interact through individual carboxyl groups, which form a closed ring and is represented by the symbol $R_4^4(12)$. As for the anhydrous form (Fig. 5b), only the single N–H···O hydrogen-bond contact exists, and the stacking patterns of the crystal structure are mainly caused by the bridging of the two H atoms of the amino group of PDA and the O atoms on the neighboring two IPA carboxyl groups, which are represented by the symbols $R_4^4(8)$ and $R_4^4(24)$. In addition, from the perspective of the crystal density, it seems that the monohydrate is supposed to be more stable. To more intuitively describe the intermolecular interactions of the two crystal forms, further analysis by the Hirshfeld surface was carried out.[50]

Hirshfeld surface analysis

HSs analysis can be employed to visualize the molecular interactions, and identify the different interaction types between the two crystal forms. Associated 2D fingerprint plots were enabled to further quantify the level of contact interactions between the molecules by highlighting their particular close contacts.[51]

The HSs maps (Fig. S3 and S4†) show the intermolecular contacts as red-colored spots, which indicate the closer contacts of the N–H···O and O–H···O hydrogen bonds. The percentage contributions of these interactions are shown on a more

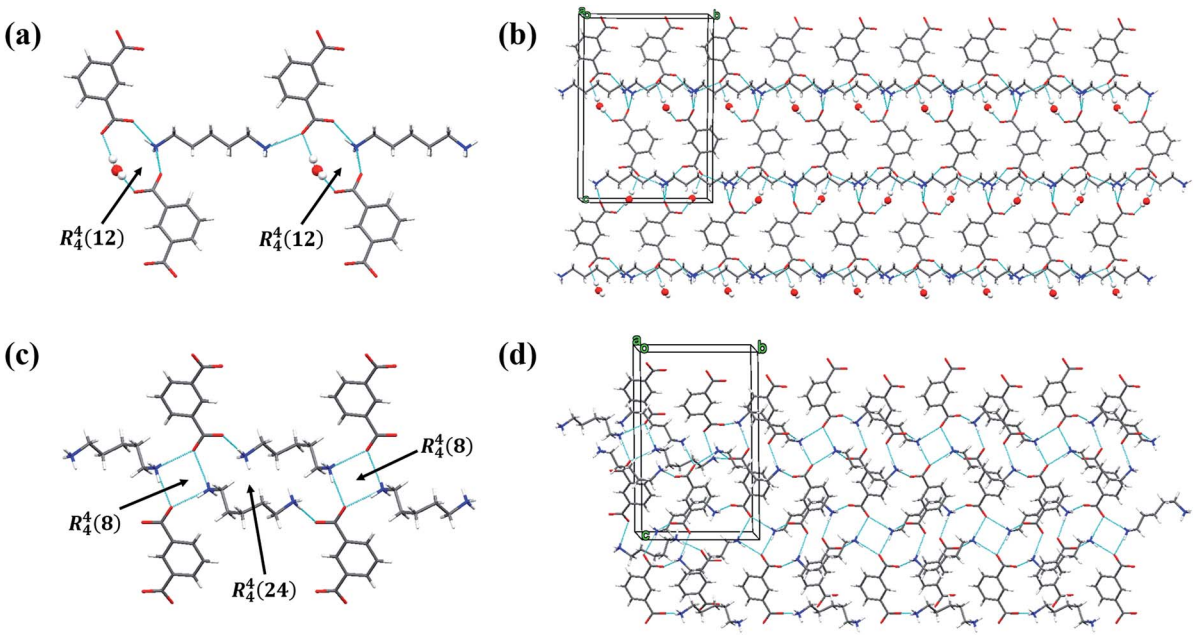

Fig. 5 (a) 2D structure and (b) 3D network of the monohydrate, and (c) 2D structure and (d) 3D network of the anhydrous form. The blue dashed line denotes the hydrogen-bonding interactions.

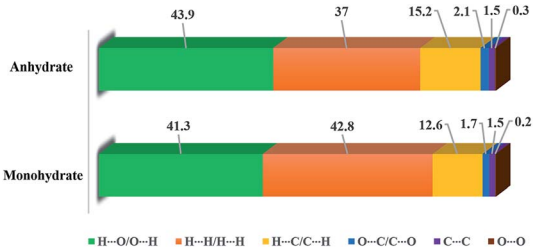

Fig. 6 Percentage contributions to the Hirshfeld surface areas for the various close intermolecular contacts for the molecules in the two forms of PDA–IPA.

quantitative basis, as displayed graphically in Fig. 6. We can see that the H···H and O···H contacts remarkably contribute the largest percentage (37.0–43.9%). In addition, the C···H interactions are another important contact, but they vary with the multicomponent specific crystal structure. The hydrogen-bond contacts that showed obvious red spots in HS were also analyzed, as shown in Fig. 7, S5 and S6.† As seen, the PDA–IPA molecules obviously show several red spots on the amino group in the anhydrate, corresponding to an amino–amino pair by N–H···O (Fig. 7b). Compared to the anhydrate, the red spots in the monohydrate are caused by the N–H···O and O–H···O hydrogen bonds together, which is due to the presence of water molecules in the crystal lattice (Fig. 7a).

The HSs analysis showed the importance of H-atom contacts and the difference of hydrogen-bond contacts in constructing the spatial packing of the two forms. Numerous H···H, O···H, and C···H interactions suggested that van der Waals interactions and hydrogen bonding play the major roles in the crystal packing.

FTIR analysis

FT-IR spectroscopy can easily complete the identification of substances containing strong hydrogen bonds, such as the N–H···O and O–H···O hydrogen bonds.[52] Fig. 8 illustrates the absorption infrared spectra of the two PDA–IPA crystal forms in the region of 550–4000 cm^{-1}. The FTIR pattern of the anhydrate has one legible characteristic peak at 1557.72 cm^{-1}, while the monohydrate has two characteristic peaks at 1561.25 and 1553.23 cm^{-1}. These absorbing peaks were both taken as the interaction of the hydrogen bond between the secondary amine N–H of PDA and the C=O group of IPA. Furthermore, when compared to anhydrate, it can be observed that there are three extra bands at 3372.95 cm^{-1}, 1658.54 cm^{-1}, and 603.97 cm^{-1} of the monohydrate, which mainly correspond to the hydroxyl group stretching vibration of the water molecules.[53] Thus, the FTIR pattern analysis can be a tool for the phase identification of two such crystal forms.

Thermal analysis

To investigate the thermal stability variation of the two crystalline forms, TGA and DSC experiments were performed. The monohydrate shows a total mass loss of 6.60%, starting at approximately 122.5 °C in the DSC curve in Fig. 9a, which corresponds to just one crystal water loss (theoretical: 6.71%). This process was also accompanied by the phase transformation from the monohydrate to anhydrous form, which was confirmed by PXRD measurements for the sample after thermal dehydration (see Fig. S7†). The anhydrate shows no weight loss before its melting point in Fig. 9b. An obvious endothermic peak occurs around 229 °C for both specimens, along with a major weight loss, which may be attributed to a combined effect of melting and decomposition. The almost same temperature onset of the endotherm indicates the identical

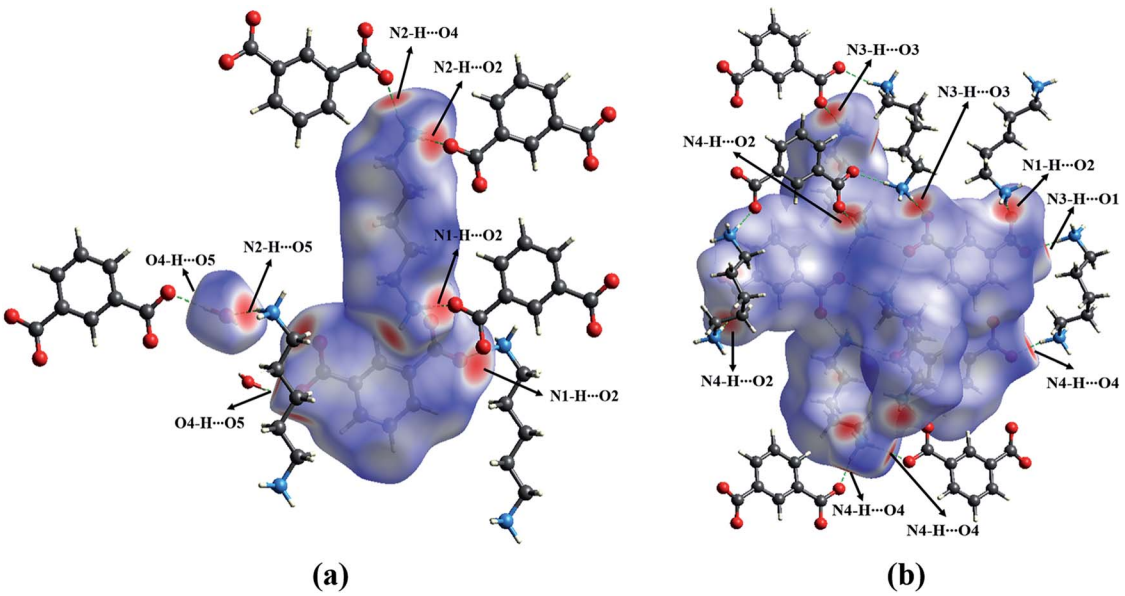

Fig. 7 The Hirshfeld surface of the two forms of PDA–IPA mapped over d_{norm} in the color range −0.7263 to 1.2573 a.u., showing the hydrogen-bond contacts with the N–H···O and O–H···O groups in the monohydrate (a) and only N–H···O in the anhydrate (b).

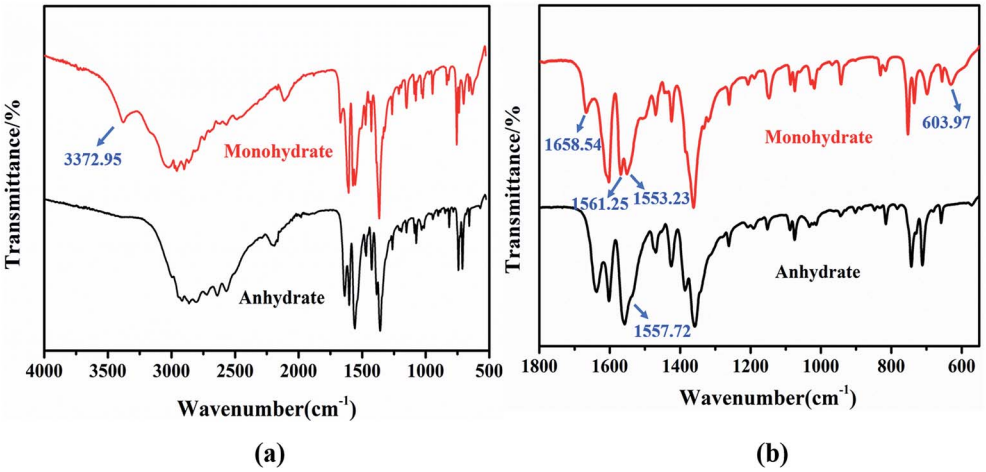

Fig. 8 Comparison of the FTIR patterns of the PDA–IPA monohydrate and anhydrate.

structures of both samples at this point as well. This phenomenon also appeared in the study of the nylon 5T monomer PDA–TPA.[49] However, the melting point of PDA–IPA is a little lower than that of PDA–TPA (T_m = 240 °C), which may be more advantageous during polymerization.

In addition, the heat of fusion values were calculated, with 134.69 kJ mol^{-1} for the monohydrate and 139.27 kJ mol^{-1} for the anhydrous form. The crystal energy of the monohydrate appeared slightly lower than that of the anhydrate, suggesting that the monohydrate is more stable in this situation.

Transitions between the monohydrate and anhydrate

The effects of temperature and relative humidity on the stability and transition between the PDA–IPA monohydrate and anhydrous phase were investigated by SST experiments, and the results are displayed in Fig. 10. Fig. 10a illustrates the influence of the two research factors on the stability of the monohydrate. When the temperature exceeds 80 °C, it can be observed that the monohydrate can be converted to the anhydrate. The crystal monohydrate appears to have favorable stability in terms of the humidity, even though the value was close to 0%. The transition from the monohydrate to anhydrous form was mainly dominated by the temperature. On the contrary, the stability of the anhydrate form was minimally affected by temperature, but extremely sensitive to the surrounding relative humidity. Fig. 10b shows that the anhydrate could be transformed to the monohydrate when the relative humidity was greater than 67%. However, the transformation phenomenon would not occur if the humidity was lower than 43%. Thus, the transformation behaviors in the SST experiments can be mainly attributed to the effect of the water activity in the environment.[54] This indicated that the transformation between the anhydrous form and monohydrate of PDA–IPA is reversible under the appropriate conditions.

The hygroscopicity experiments of the monohydrate and anhydrous forms of PDA–IPA subjected to various surrounding humidity values were further performed at room temperature, and the results can be seen in Fig. S8.† When the relative humidity was 67% or less, it showed that the two crystalline solid powders were stable. When it was 76%, both forms indicated slight moisture absorption. Finally, when it reached up to 98%, obvious moisture absorption can be observed, but the crystal structure was still unexpectedly stable in this case.

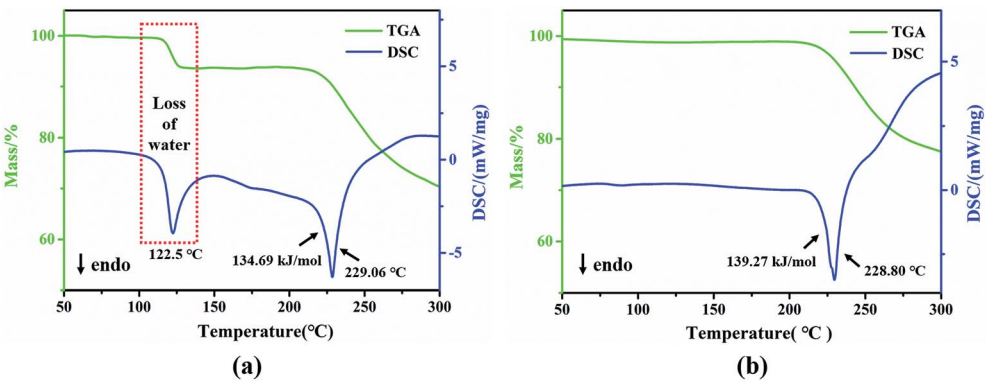

Fig. 9 TGA and DSC curves of the monohydrate (a) and anhydrate (b) of PDA–IPA.

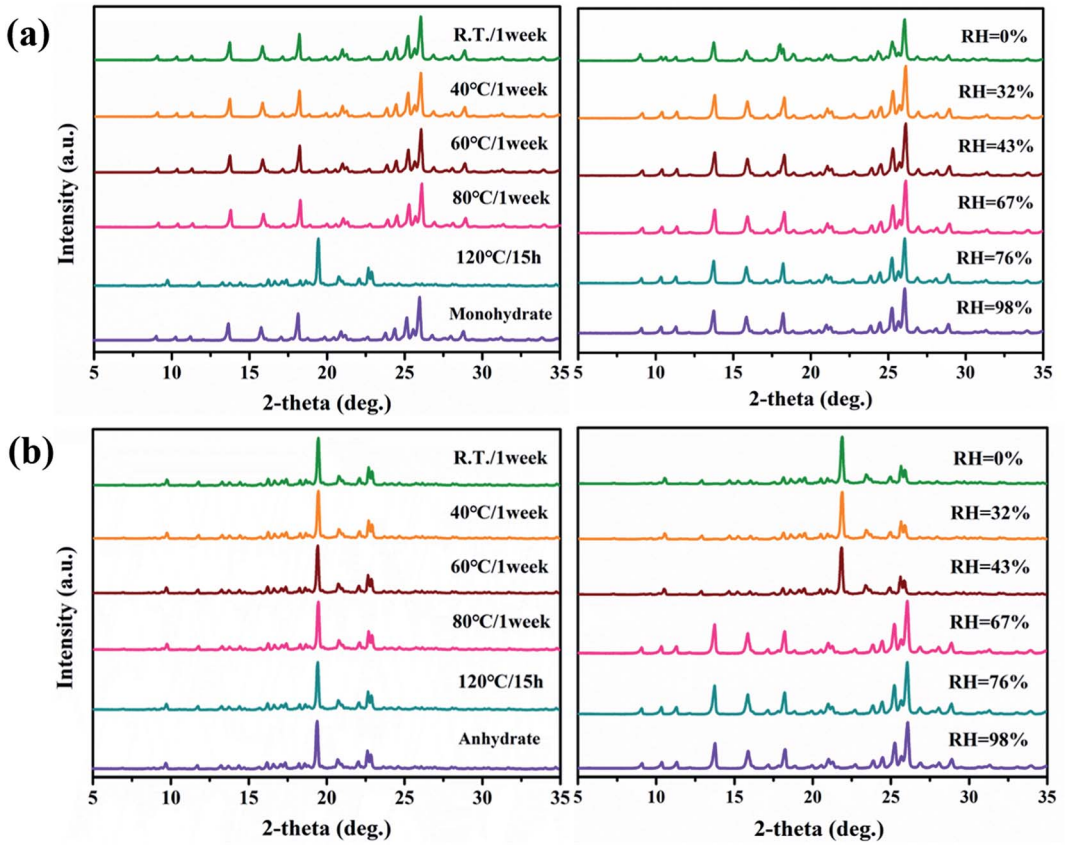

Fig. 10 The SST process of the monohydrate (a) and anhydrate (b) under different temperature and humidity conditions.

In order to clarify the effect of the solvent on the phase transition and explore whether there are new unknown crystal forms, the experiments of solvent-mediated transformation in different pure solvents or binary organic–water mixtures were also carried out. The findings are illustrated in Fig. 11. Fig. 11a and b shows us that no new polymorphs occur under the test conditions, except for a phase transformation between the monohydrate and anhydrate. The hydrate was the preferential structure in the system of water participation. To further shed light on the influence mechanism of temperature and water activity on the relative stability and transformation of the two crystal forms of PDA–IPA under various thermodynamic conditions, a slurry experiment in a water–ethanol binary system was designed and performed.

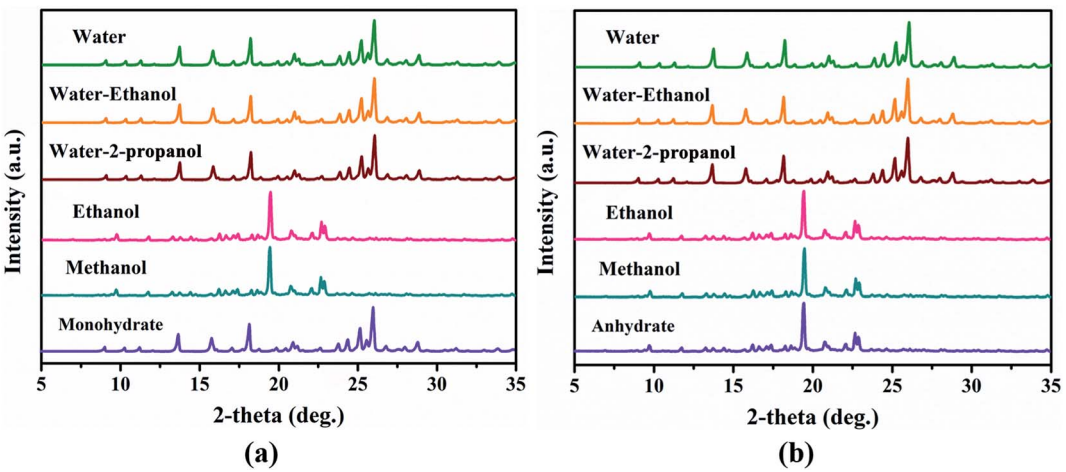

Fig. 11 The SMPT profiles for the monohydrate (a) of PDA–IPA, and its anhydrate (b) in different solvents. The ratio in the binary solvent system is 1 : 1 (v : v).

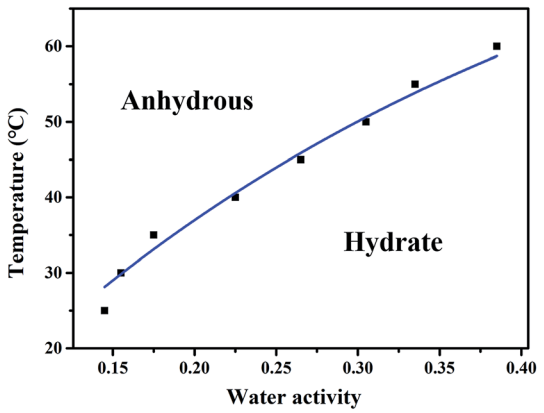

Fig. 12 Water activity–temperature phase diagram of the PDA–IPA monohydrate and anhydrous form, which determined the boundary of transformation between the hydrate and anhydrous zones.

The phase diagram after equilibration for 24 h was measured to investigate the dependence of PDA–IPA on the water activity (a_w) in ethanol/water mixtures during the hydration process at different temperatures. The results were displayed in Fig. 12. At 25 °C, if the value of a_w was lower than 0.14, the anhydrate was the favorable form at equilibrium, whereas the monohydrate appeared to be more stable if the value was more than 0.15. The area of the anhydrous zone was narrow, and the hydrate zone was rather widespread in this case (the phase diagram of the water activity–temperature conversion at ambient temperature is shown in Fig. S9 and S10†). However, at 60 °C, the anhydrate was the stable form if the value of a_w was less than 0.38, whereas the monohydrate will be more stable if the value was more than 0.39. Notably, the value of the transition temperature of the two forms can be significantly affected by the water activity, showing a clear trend of rising with the increase of the water activity. With increasing water activity, the transition temperature from the anhydrate to monohydrate form increases. Meanwhile, we can see that the anhydrous zone of the PDA–IPA crystals is relatively narrow compared with its hydrate zone. In addition, the trend became more noticeable as the temperature and water activity increased.

Conclusions

In this contribution, we found that PDA–IPA exists in two crystal forms. One is the rod-like orthorhombic monohydrate, and the other form is the block-like monoclinic anhydrate. We investigated their crystal structures, thermal properties, stabilities, transformation behaviors, as well as their conversion mechanisms by SCXRD, PXRD, FT-IR, TGA-DSC, and transformation experiments.

The huge difference in the crystal structure conformation of the monohydrate and anhydrous phases, which leads to their distinct hydrogen bonding modes and intermolecular interactions. There are two types of dominant hydrogen-bond contacts, N–H···O and O–H···O, in the monohydrate. Conversely, the anhydrate form only has the N–H···O interaction. The Hirshfeld surface analysis shows the differences clearly between the two forms of PDA–IPA to study their structure–property relationships. Moreover, the water loss of the monohydrate leads to the changes in packing and conformation, which are critical to the transformation into the anhydrous form.

The relative stability relationship between the two forms was further established. The stability of the monohydrate form against hygroscopicity was proved to be higher than that of the anhydrous phase. The transformation from the monohydrate to the anhydrate was mainly dominated by the temperature in the direct solid–solid transformation experiments. However, the conversion from the anhydrate to hydrate was hardly influenced by the temperature, but more sensitive to the surrounding relative humidity. Besides, it was found that the phase transition between the two crystal forms depends strongly on the temperature and water activity. Through the water activity–temperature phase diagram, the zones where the two crystalline forms can exist in stable forms were determined. The results presented in this work could give some meaningful instructions for the control preparation of the target crystal form of PDA–IPA, and offer the high-quality monomer for the bio-based nylon 5I.

Conflicts of interest

The authors declare that there is no conflict of interest.

Acknowledgements

This work was supported by the National Natural Science Foundation of China (NSFC 21908100), the Jiangsu Synergetic Innovation Center for Advanced Bio-Manufacture (XTE1847), the Key R&D Plan of Jiangsu Province (BE2019001) and National Key Research and Development Program of China (2019YFD1101202, 2019YFD1101204).

References

1 B. Liu, G. Hu, J. Zhang and W. Yan, Non-isothermal crystallization, yellowing resistance and mechanical properties of heat-resistant nylon 10T/66/titania dioxide/glass fibre composites, *RSC Adv.*, 2019, **9**(13), 7057–7064.
2 T. F. Novitsky, C. A. Lange, L. J. Mathias, S. Osborn, R. Ayotte and S. Manning, Eutectic melting behavior of polyamide 10,T-co-6,T and 12,T-co-6,T copolyterephthalamides, *Polymer*, 2010, **51**(11), 2417–2425.
3 Y. J. Kim, K. E. Yohana, H. S. Lee and J. Kim, Solid-State Polymerization of Semiaromatic Copolyamides of Nylon-4,T and Nylon-4,6: Composition Ratio Effect and Thermal Properties, *Ind. Eng. Chem. Res.*, 2012, **51**(49), 15801–15810.
4 R. J. Gaymans and A. G. J. V. d. Ham, Nylon 4,I: an amorphous polyamide, *Polymer*, 1984, **25**, 1755.
5 M. Firdaus and M. A. R. Meier, Renewable polyamides and polyurethanes derived from limonene, *Green Chem.*, 2013, **15**, 370–380.
6 K. Hashimoto, N. Hashimoto, T. Kamaya, J. Yoshioka and H. Okawa, Synthesis and properties of bio-based

polyurethanes bearing hydroxy groups derived from alditols, *J. Polym. Sci., Part A: Polym. Chem.*, 2011, **49**(4), 976–985.

7 T. A. Osswald and S. García-Rodríguez, History of sustainable bio-based polymers, *Green Chem.*, 2011, 1–21.

8 P. Yang, X. Li, H. Liu, Z. Li, J. Liu, W. Zhuang, J. Wu and H. Ying, Thermodynamics, crystal structure, and characterization of a bio-based nylon 54 monomer, *CrystEngComm*, 2019, **21**(46), 7069–7077.

9 D. S. Ogunniyi, Castor oil: a vital industrial raw material, *Bioresour. Technol.*, 2006, **97**(9), 1086–1091.

10 S. H. Hong, J. S. Kim, S. Y. Lee, Y. H. In, S. S. Choi, J. K. Rih, C. H. Kim, H. Jeong, C. G. Hur and J. J. Kim, The genome sequence of the capnophilic rumen bacterium Mannheimia succiniciproducens, *Nat. Biotechnol.*, 2004, **22**(10), 1275–1281.

11 J. Bosch, Modeling Techniques for Measuring Galaxy Properties in Multi-Epoch Surveys, *J. Bus. Strat.*, 2011, **35**(6), 49–57.

12 D. J. Burke, T. Kawauchi, M. J. Kade, F. A. Leibfarth, B. McDearmon, M. Wolffs, P. H. Kierstead, B. Moon and C. J. Hawker, Ketene-Based Route to Rigid Cyclobutanediol Monomers for the Replacement of BPA in High Performance Polyesters, *ACS Macro Lett.*, 2012, **1**(11), 1228–1232.

13 B. Bechtloff, S. Nordhoff and J. Ulrich, Pseudopolymorphs in industrial use, *Cryst. Res. Technol.*, 2015, **36**(12), 1315–1328.

14 P. A. Basford, K. R. Back, M. Cram, R. Docherty, R. J. Davey and A. J. Cruz-Cabeza, Impact of Crystal Structure and Molecular Conformation on the Hydration Kinetics of Fluconazole, *Cryst. Growth Des.*, 2019, **19**(12), 7193–7205.

15 P. Cui, Q. Yin, Y. Guo and J. Gong, Polymorphic Crystallization and Transformation of Candesartan Cilexetil, *Ind. Eng. Chem. Res.*, 2012, **51**(39), 12910–12916.

16 H. G. Brittain, *Polymorphism in Pharmaceutical Solids*, Informa Healthcare, New York, 1999, vol. 192.

17 K. Fujii, M. Aoki and H. Uekusa, Solid-State Hydration/Dehydration of Erythromycin A Investigated by Ab Initio Powder X-ray Diffraction Analysis: Stoichiometric and Nonstoichiometric Dehydrated Hydrate, *Cryst. Growth Des.*, 2013, **13**(5), 2060–2066.

18 Z. Liu, Q. Yin, X. Zhang, J. Gong and C. Xie, Characterization and Structure Analysis of Cefodizime Sodium Solvates Crystallized from Water and Ethanol Binary Solvent Mixtures, *Ind. Eng. Chem. Res.*, 2014, **53**(8), 3373–3377.

19 S. SeethaLekshmi, M. S. R. N. Kiran, U. Ramamurty and S. Varughese, Phase Transitions and Anisotropic Mechanical Response in a Water-rich Trisaccharide Crystal, *Cryst. Growth Des.*, 2020, **20**(1), 442–448.

20 F. Liu, D. E. Hooks, N. Li, N. A. Mara and J. A. Swift, Mechanical Properties of Anhydrous and Hydrated Uric Acid Crystals, *Chem. Mater.*, 2018, **30**(11), 3798–3805.

21 W. Du, Q. Yin, H. Hao, Y. Bao, X. Zhang, J. Huang, X. Li, C. Xie and J. Gong, Solution-Mediated Polymorphic Transformation of Prasugrel Hydrochloride from Form II to Form I, *Ind. Eng. Chem. Res.*, 2014, **53**(14), 5652–5659.

22 R. R. E. Steendam, U. B. R. Khandavilli, L. Keshavarz and P. J. Frawley, Solution versus Crystal Hydration: The Case of γ-Amino Acid Pregabalin, *Cryst. Growth Des.*, 2019, **19**, 4483–4488.

23 M. Sacchetti, Determining the relative physical stability of anhydrous and hydrous crystal forms of GW2016, *Int. J. Pharm.*, 2004, **273**(1–2), 195–202.

24 Y. Li, P. S. Chow, R. B. H. Tan and S. N. Black, Effect of Water Activity on the Transformation between Hydrate and Anhydrate of Carbamazepine, *Org. Process Res. Dev.*, 2008, **12**(2), 264–270.

25 X. Zhang, Q. Yin, W. Du, J. Gong, Y. Bao, M. Zhang, B. Hou and H. Hao, Phase Transformation between Anhydrate and Monohydrate of Sodium Dehydroacetate, *Ind. Eng. Chem. Res.*, 2015, **54**(13), 3438–3444.

26 H. Grünewald, Book Review: The Merck Index. An Encyclopedia of Chemicals and Drugs, *Angew. Chem., Int. Ed.*, 1969, **8**(1), 86–87.

27 J. Boeckmann and C. Näther, Solid-state transformation of $[Co(NCS)_2(pyridine)_4]$ into $[Co(NCS)_2(pyridine)_2]_n$: from Curie-Weiss paramagnetism to single chain magnetic behaviour, *Dalton Trans.*, 2010, **39**(45), 11019–11026.

28 D. C. Souza, V. Pralong, A. J. Jacobson and L. F. Nazar, A reversible solid-state crystalline transformation in a metal phosphide induced by redox chemistry, *Science*, 2002, **296**(5575), 2012–2015.

29 F. Liu, F. Sommer, C. Bos and E. J. Mittemeijer, Analysis of solid state phase transformation kinetics: models and recipes, *Metall. Rev.*, 2007, **52**(4), 193–212.

30 F. Zou, Q. Chen, P. Yang, J. Zhou, J. Wu, W. Zhuang and H. Ying, Solution-Mediated Polymorphic Transformation: From Amorphous to Crystals of Disodium Guanosine 5′-Monophosphate in Ethanol, *Ind. Eng. Chem. Res.*, 2017, **56**, 8274–8282.

31 D. L. T. Nguyen and K.-J. Kim, Solvent-Mediated Polymorphic Transformation of α-Taltirelin by Seeded Crystallization, *Chem. Eng. Technol.*, 2016, **39**(7), 1281–1288.

32 A. Maher, C. C. Seaton, S. Hudson, D. M. Croker, Å. C. Rasmuson and B. K. Hodnett, Investigation of the Solid-State Polymorphic Transformations of Piracetam, *Cryst. Growth Des.*, 2012, **12**, 6223–6233.

33 A. Maher, D. M. Croker, C. C. Seaton, Å. C. Rasmuson and B. K. Hodnett, Solution-Mediated Polymorphic Transformation: Form II to Form III Piracetam in Organic Solvents, *Cryst. Growth Des.*, 2014, **14**, 3967–3974.

34 L. Chee-wei Jennifer and W. R. Ronald, Solubilities of and Transformations between the Anhydrous and Hydrated Forms of L-Serine in Water–Methanol Solutions, *Cryst. Growth Des.*, 2006, **6**(8), 1808–1812.

35 S. Maruyama, H. Ooshima and J. Kato, Crystal structures and solvent-mediated transformation of Taltireline polymorphs, *Chem. Eng. J.*, 1999, **75**(3), 193–200.

36 R. Mohan, K. K. Koo, C. Strege and A. S. Myerson, Effect of Additives on the Transformation Behavior of l-Phenylalanine in Aqueous Solution, *Ind. Eng. Chem. Res.*, 2001, **40**(26), 6111.

37 P. Yang, C. Lin, W. Zhuang, Q. Wen, F. Zou, J. Zhou, J. Wu and H. Ying, Insight into a direct solid–solid

transformation: a potential approach for the removal of residual solvents, *CrystEngComm*, 2016, **18**, 1699–1704.

38 Z. Ding, W. Su, X. Huang, B. Tian, X. Cheng, Y. Mao, G. Li, H. Liu and H. Hao, Understanding the Role of Water in Different Solid Forms of Avibactam Sodium and Its Affecting Mechanism, *Cryst. Growth Des.*, 2020, **20**(2), 1150–1161.

39 Bruker, *SAINT and SMART-1000*, Bruker AXS Inc., Madison, Wisconsin, USA, 2012.

40 G. M. Sheldrick, SHELXT – Integrated space-group and crystal-structure determination, *Acta Crystallogr.*, 2015, **71**(1), 3–8.

41 I. Usón and G. M. Sheldrick, An introduction to experimental phasing of macromolecules illustrated by SHELX: new autotracing features, *Acta Crystallogr.*, 2018, **74**(2), 106.

42 A. L. Spek, Single-crystal structure validation with the program PLATON, *J. Appl. Crystallogr.*, 2003, **36**(1), 7–13.

43 A. Gavezzotti and G. Filippini, Geometry of the Intermolecular X-H.cntdot..cntdot..cntdot.Y (X, Y = N, O) Hydrogen Bond and the Calibration of Empirical Hydrogen-Bond Potentials, *J. Phys. Chem.*, 1994, **98**, 4831–4837.

44 F. L. Hirshfeld, Bonded-atom fragments for describing molecular charge densities, *Theor. Chim. Acta*, 1977, **44**(2), 129–138.

45 M. J. Turner; J. J. McKinnon; S. K. Wolff; D. J. Grimwood; P. R. Spackman; D. Jayatilaka and M. A. Spackman, *CrystalExplorer17*, The University of Western Australia, 2017.

46 M. A. Spackman and J. J. McKinnon, Fingerprinting intermolecular interactions in molecular crystals, *CrystEngComm*, 2002, **4**, 378–392.

47 P. Yang, X. Li, H. Liu, Z. Li, J. Liu, W. Zhuang, J. Wu and H. Ying, Thermodynamics, crystal structure, and characterization of a bio-based nylon 54 monomer, *CrystEngComm*, 2019, **21**, 7069–7077.

48 P. Yang, X. Peng, S. Wang, D. Li, M. Li, P. Jiao, W. Zhuang, J. Wu, Q. Wen and H. Ying, Crystal structure, thermodynamics, and crystallization of bio-based polyamide 56 salt, *CrystEngComm*, 2020, **22**, 3234–3241.

49 Z. Li, P. Yang, H. Liu, J. Liu, S. Zhu, X. Li, W. Zhuang, J. Wu and H. Ying, Crystal forms and phase transformation of 1,5-pentanediamine-terephthalate: a bio-based nylon 5T monomer, *Acta Crystallogr., Sect. B: Struct. Sci., Cryst. Eng. Mater.*, 2020, **76**, 524–533.

50 M. A. Spackman and D. Jayatilaka, Hirshfeld surface analysis, *CrystEngComm*, 2009, **11**(1), 19–32.

51 X. Zhang, L. Zhou, C. Wang, Y. Li, Y. Wu, M. Zhang and Q. Yin, Insight into the role of hydrogen bonding playing in the molecular self-assembly process of sulfamethazine solvates, *Cryst. Growth Des.*, 2017, **17**, 6151–6157.

52 A. M. Tudor, S. J. Church, P. J. Hendra, M. C. Davies and C. D. Melia, The Qualitative and Quantitative Analysis of Chlorpropamide Polymorphic Mixtures by Near-Infrared Fourier Transform Raman Spectroscopy, *Pharm. Res.*, 1993, **10**(12), 1772–1776.

53 C. S. Jamieson, A. M. Mebel and R. I. Kaiser, Understanding the Kinetics and Dynamics of Radiation-induced Reaction Pathways in Carbon Monoxide Ice at 10 K, *Astrophys. J., Suppl. Ser.*, 2006, **163**(1), 184–206.

54 H. Qu, M. Louhi-Kultanen, J. Rantanen and J. Kallas, Solvent-Mediated Phase Transformation Kinetics of an Anhydrate/Hydrate System, *Cryst. Growth Des.*, 2006, **6**(9), 2053–2060.

